crystals

MDPI

Article

Crystal Growth of Quantum Magnets in the Rare-Earth Pyrosilicate Family $R_2Si_2O_7$ (R = Yb, Er) Using the Optical Floating Zone Method

Harikrishnan S. Nair [1,2], Tim DeLazzer [1], Tim Reeder [1], Antony Sikorski [1], Gavin Hester [1] and Kate A. Ross [1,*]

[1] Department of Physics, Colorado State University, 200 W. Lake St., Fort Collins, CO 80523-1875, USA; delazzer@rams.colostate.edu (T.D.); treeder5@jhu.edu (T.R.); antony.sikorski@gmail.com (A.S.); Gavin.Hester@colostate.edu (G.H.)

[2] Department of Physics, 500 W. University Ave, The University of Texas at El Paso, El Paso, TX 79968, USA; hnair@utep.edu

* Correspondence: Kate.Ross@colostate.edu; Tel.: +1-970-491-5370

Received: 23 March 2019; Accepted: 2 April 2019; Published: 7 April 2019

Abstract: We report on the crystal growth of rare-earth pyrosilicates, $R_2Si_2O_7$ for R = Yb and Er using the optical floating zone method. The grown crystals comprise members from the family of pyrosilicates where the rare-earth atoms form a distorted honeycomb lattice. C-$Yb_2Si_2O_7$ is a quantum dimer magnet with field-induced long range magnetic order, while D-$Er_2Si_2O_7$ is an Ising-type antiferromagnet. Both growths resulted in multi-crystal boules, with cracks forming between the different crystal orientations. The $Yb_2Si_2O_7$ crystals form the C-type rare-earth pyrosilicate structure with space group $C2/m$ and are colorless and transparent or milky white, whereas the Er-variant is D-type, $P2_1/b$, and has a pink hue originating from Er^{3+}. The crystal structures of the grown single crystals were confirmed through a Rietveld analysis of the powder X-ray diffraction patterns from pulverized crystals. The specific heat of both C-$Yb_2Si_2O_7$ and D-$Er_2Si_2O_7$ measured down to 50 mK indicated a phase transition at $T_N \approx 1.8$ K for D-$Er_2Si_2O_7$ and a broad Schottky-type feature with a sharp anomaly at 250 mK in an applied magnetic field of 0.8T along the c-axis in the case of C-$Yb_2Si_2O_7$.

Keywords: optical floating zone method; rare-earth pyrosilicates; $Yb_2Si_2O_7$; $Er_2Si_2O_7$; quantum dimer magnet; Ising antiferromagnet

1. Introduction

The rare-earth pyrosilicates, $R_2Si_2O_7$ where R is a rare-earth element, were studied in the past owing to the polymorphism that these compounds displayed as a function of temperature and the ionic size of the rare-earth R^{3+} [1]. Depending on the temperature of the synthesis and the ionic radius, seven different crystal types were previously identified. Figure 1 (left) illustrates the conditions required to stabilize the seven crystal types designated using the capital letters A, B, C, D, E, F, G. These structure types were assigned in the original work by Felsche et al. [1] where the phase diagram in the temperature range 900 °C to 1800 °C is shown for the different rare-earths.

The structure type-A is tetragonal having the space groups $P4_122$ or $P4_1$. The pyrosilicates $La_2Si_2O_7$, $Pr_2Si_2O_7$, $Nd_2Si_2O_7$, $Sm_2Si_2O_7$ and $Eu_2Si_2O_7$ belong to this type. The structures type-B and type-F are triclinic having the space groups $P\bar{1}$ or $P1$. The compounds $Eu_2Si_2O_7$, $Gd_2Si_2O_7$, $Tb_2Si_2O_7$, $Dy_2Si_2O_7$, $Ho_2Si_2O_7$ and $Er_2Si_2O_7$ can stabilize this polymorph. The structure type-C is monoclinic having the space group symmetry $C2/m$. The compounds $Yb_2Si_2O_7$ and $Er_2Si_2O_7$ that form the focus of the present paper can crystallize in C-type structure similar to $Ho_2Si_2O_7$, $Tm_2Si_2O_7$ and $Lu_2Si_2O_7$.

Note that several silicate compounds have polymorphs of the structure types A→G. Among the other structure types, type-E is orthorhombic (*Pnma* and $Pna2_1$), type-D is monoclinic ($P2_1/a$) and type-G is psuedo-orthorhombic ($P2_1/n$).

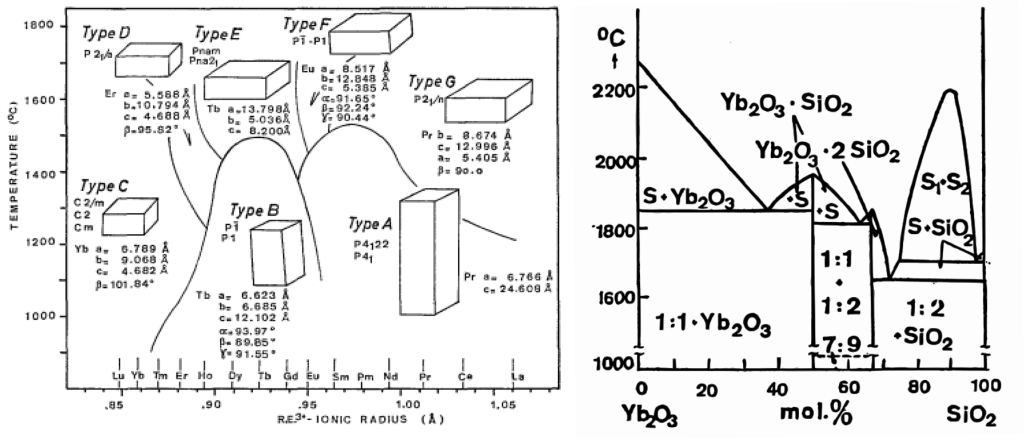

Figure 1. (**left**) Different crystal phases that are allowed in the rare-earth silicate family of $R_2Si_2O_7$ compounds. Note that for R = Yb only C-type is available. For Er, synthesis below T = 1400 °C results in the C-type whereas the D-type is stabilized if high-temperature synthesis is employed. (**Right**) The binary phase diagram of Yb_2O_3-SiO_2. The 1:2 mol% corresponding to $Yb_2Si_2O_7$ is indicated. Both the figures are reproduced from Ref. [1].

The majority of the rare-earth pyrosilicates were originally investigated to understand their performance as scintillation crystals in gamma ray or X-ray detectors, or as host materials for optically-active rare-earths [2–4]. Recently, the rare-earth pyrosilicates were investigated to understand their thermal expansion coefficients, which are beneficial from the perspective of environmentally benign thermal barrier coatings [5]. Structurally, switchable negative contribution from low-frequency phonons to thermal expansion was found from studying the localized lattice distortions in C-$Yb_2Si_2O_7$ and related compounds. Though single crystals of several rare-earth pyrosilicates, $R_2Si_2O_7$ (R = Tm, Er, Ho, Dy), have been prepared via flux growth [6,7], detailed studies on the magnetism of the rare-earth lattice forming a distorted honeycomb structure in these compounds are lacking and, in particular, the crystals prepared by flux method are not large enough for neutron scattering investigations. Initial studies on the magnetic properties of D-$Er_2Si_2O_7$ had identified a magnetic phase transition at 1.9 K and the associated Ising-like magnetic behavior after analyzing the g-tensors estimated from magnetic susceptibility analysis on flux-grown single crystals [8]. Single crystals and ceramics of $Er_2Si_2O_7$ were studied in detail using X-ray investigations to clearly document the phase transitions between different structure types ($P1 \rightarrow C2/m \rightarrow P2_1/b$) as a function of synthesis temperature [7,9]. Meanwhile C-$Yb_2Si_2O_7$ was previously synthesized using solid-state reactions in order to study the thermal expansion and thermal conductivity at high temperatures, 473 K to 1573 K [10]. C-$Yb_2Si_2O_7$ powders were also synthesized using sol-gel method using ytterbium nitrate and tetraethyl orthosilicate as starting materials [11]. Large, clear single crystal pieces (≈15 mm) of C-$Yb_2Si_2O_7$ were prepared from micro-pulling-down (μ-PD) technique to fabricate components for near-infra red scintillators in medical applications [12]. While studies on magnetic properties of $Yb_2Si_2O_7$ were non-existent until the recent discovery of quantum dimer magnet by our group [13], the electronic structure of C-$Yb_2Si_2O_7$ has been studied in brief using X-ray photoemission spectroscopy [14] and valence electron energy-loss spectroscopy [15]. The existence of an isolated energy level in the band gap of $Yb_2Si_2O_7$ was identified in the latter report.

The present work fills the lacuna in the literature on Yb and Er-based $R_2Si_2O_7$ related to the single crystal preparation using the optical floating zone method. We also demonstrate the magnetic properties of the samples via their low-temperature specific heats. The crystals obtained by this method

are suitable for single crystal neutron scattering investigations, the first of which have recently been carried out by our group [13].

2. Crystal Growth Using Optical Floating Zone Method

In the present work, single crystals of C-$Yb_2Si_2O_7$ and D-$Er_2Si_2O_7$ are grown using the optical floating zone method which is known for producing high quality oxide crystals. An infrared furnace procured from Crystal Systems Inc. (Massachusetts, United States, model FZ-T-10000-H-VIII-VPO-PC) was used for the single crystal growth. High-purity starting materials of Yb_2O_3, Er_2O_3 and SiO_2 (Sigma Aldrich, Missouri, United States, 99.99% purity) were used to prepare polycrystalline powder materials of $Yb_2Si_2O_7$ and $Er_2Si_2O_7$. The rare-earth oxides Yb_2O_3 and Er_2O_3 were calcined at 950 °C in order to remove the moisture prior to synthesis of ceramic starting materials. After this procedure, the precursor oxides were weighed according to the stoichiometry (R_2O_3:SiO_2 = 1:2) and mixed together thoroughly. In the case of $Yb_2Si_2O_7$, wet-grinding was performed with the aid of methanol. After the mixing, the $Yb_2Si_2O_7$ powders were heated in re-crystallized alumina crucibles, at T = 1350 °C and subsequently at T = 1420 °C several times until the phase formation was confirmed using X-ray diffraction. In the case of $Er_2Si_2O_7$ the precursors were mixed together and the first sintering was carried out at 1400 °C for 48 h; the second and the third at 1500 °C for 48 h, and the fourth at 1500 °C for 36 h. During the powder synthesis of $Yb_2Si_2O_7$ and $Er_2Si_2O_7$, we found that $(Yb/Er)_2SiO_5$ was a common sample impurity, which was found to be more prominent in X-ray powder diffraction of the surface material compared to the bulk. This was taken care of by sintering the silicates as dense pellets. Once the phase formation was confirmed, the powders were compacted into ingots for crystal growth by filling them in rubber balloons and applying a hydrostatic pressure of 70 MPa. Ingots thus prepared were again sintered in alumina boats at T = 1400 °C to ensure strength and to facilitate initial grain growth. The resulting ceramic rod densities were estimated to be 79% for $Er_2Si_2O_7$ and typically 80% for $Yb_2Si_2O_7$.

Several attempts were made to grow a single crystal of $Yb_2Si_2O_7$ using the conventional floating zone technique (FZ) or the traveling-solvent floating zone technique (TSFZ) using a pellet of SiO_2:Yb_2O_3::70%:30% as solvent. The successful attempts are described in detail in the following paragraph, and the crystal growth parameters are collected in Table 1. In one of the early attempts, we performed a growth experiment using feed and seed rods prepared from powder of $Yb_2Si_2O_7$ which was not completely reacted to form a pure phase. We call the crystal grown from this batch H015. The crystal growth was performed using 4 × 1.5 kW halogen lamps and flowing air at 5 L/min. The feed and the seed rods were rotated at 32 rpm and 28 rpm, respectively. We observed that melting started at 72.8% of lamp voltage. The voltage of the lamps were later stabilized at 75% and crystal growth rate set at 6 mm/h. Although a high growth rate of 12 mm/h was experimented with for a while, it did not lead to a stable molten zone and hence, the growth rate was reverted to 6 mm/h. In this way, a 53.5 mm multi-crystal boule was grown. However, it was noticed that the melt in the hot-zone reduced in volume over time and subsequently the feed rod had to be lowered to the zone several times. Growth trials were performed with different growth rates ranging from 1.5 mm/h to 10 mm/h. Back-feeding of the feed rod was also used to control the zone in several trials. However, a perfectly stable zone was not attained in our trials. The grown crystal of H015 had different regions where it was milky white and transparent. The crystal was, however, severely cracked. The cracks in the boule separated different domains of crystal grown in to a multi-crystal. The transparent regions were found to be of good quality through Laue photographs.

Table 1. The details of the growth parameters that were used in the successful optical floating zone crystal growth of $Yb_2Si_2O_7$ and $Er_2Si_2O_7$ pyrosilicates. The $Yb_2Si_2O_7$ crystals are H015, H037, H045. The $Er_2Si_2O_7$ crystal is T01. †: in this case back-feeding at 1.5 mm/h was used.

Growth Parameters	H015	H037	H045	T01
Starting material	semi-reacted ingot	reacted ingot	reacted ingot	reacted ingot
Method	FZ	TSFZ	FZ	FZ
Lamp voltage (%V)	75% (4 × 1.5 kW)	73.5% (4 × 1.5 kW)	75.2% (4 × 1.5 kW)	68.8% (4 × 1 kW)
Lamp used	1.5 kW	1.5 kW	1.5 kW	1 kW
Ambiance	air	O_2	air	O_2
Pressure	1 atm	1 atm	1 atm	1 atm
Flow rate	5 L/m	0 L/m	2 L/m	0.35 L/min
Growth rate	6 mm/h	3 mm/h †	7 mm/h †	7 mm/h
Feed/Seed rotation	32/28 rpm	20/20 rpm	25/25 rpm	20/20 rpm
Grown length	60 mm	65 mm	53 mm	33 mm
Color of crystal	whitish	transparent	whitish	pink

For the subsequent growth experiment, a new feed rod was prepared starting from fresh reactants and forming phase pure $Yb_2Si_2O_7$, named H037(Figure 2). We attempted the traveling-solvent floating zone method. A solvent pellet of 70:30 mol% SiO_2:Yb_2O_3 was used in the TSFZ type of crystal growth [16] as an attempt to lower the melting point (following the liquidus curve in Figure 1 to lower mol% SiO_2) so as to potentially reduce the cracking problem that lead to multi-crystals in the previous attempt. The growth atmosphere was O_2 at a static pressure of 1 atm. The feed and the seed rods were counter-rotated at 20 rpm. However, at the beginning of the growth, the solvent was observed to significantly shrink in size and melt at 71.4%. The ingots started to melt at 72% and the growth commenced at a rate of 3 mm/h. Similar to the previous case of H015, reduction in melt volume was observed for H037 as well and hence, a back-feeding of the feed ingot was administered at the rate of 0.5 mm/h. A mostly transparent crystal of length 65 mm was grown. Post-growth, a faint whitish deposit was observed on the inside surface of the quartz tube which only produced an amorphous response in X-ray diffraction and hence was not phase-identified. The deposit is most likely SiO_2 that evaporated from the molten zone and deposited on the inside of the quartz tube. Using higher pressure of oxygen in the growth chamber to control the vapor pressure might help in reducing the preferential loss of one component from the melt leading to destabilizing of zone.

A third successful attempt was made with a new batch of feed rod from phase pure $Yb_2Si_2O_7$ powder, H045. For this growth, the ambiance was flowing atmospheric air at the rate of 2 L/m. The feed and the seed rods were rotated at 25 rpm. Initially, the ingots melted at 72% and the growth rate was set to 5 mm/h with back-feeding of 0.5 mm/h. After about 3 h, lamp voltage was at 75.2% and growth rate had been increased to 7 mm/h which lead to a stable growth condition. A whitish crystal of 53 mm length was grown. Cracks were reduced this time but the crystal had mainly two large cracks and was found to be a multi-crystal, with three crystal grains which grew together along the long axis of the growth. Hence, the stable growth rate for C-$Yb_2Si_2O_7$ was optimized at 7 mm/h in the ambiance of flowing air. The largest crystal piece obtained for C-$Yb_2Si_2O_7$ was about 0.3 g (8 mm × 3 mm × 2 mm).

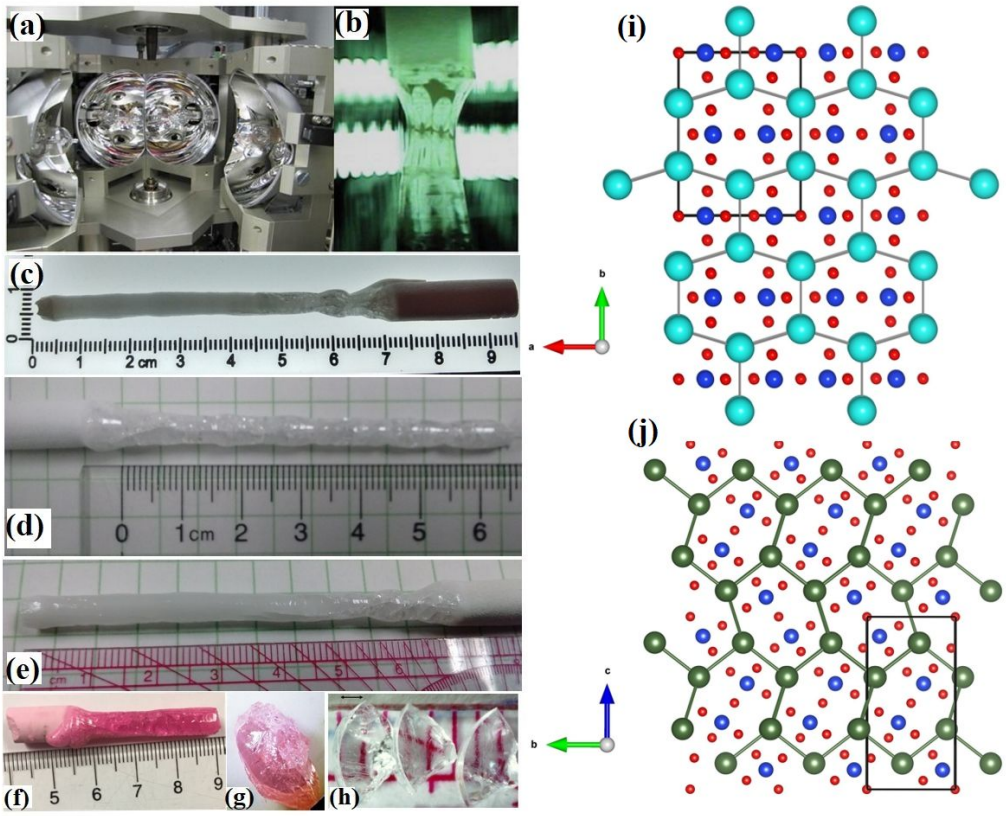

Figure 2. (**a**) The 4-hemiellipsoidal lamp and mirror arrangement of the optical floating zone growth chamber. (**b**) The molten zone stabilized between the seed and the feed ingots in the case of H015. (**c**–**e**) The C-$Yb_2Si_2O_7$ crystals grown using the optical floating zone method: labeled respectively as H015, H037 and H045. (**f**) The as-grown crystal boule of D-$Er_2Si_2O_7$. (**g**) A piece of crystal of D-$Er_2Si_2O_7$ shown under a microscope. (**h**) Clear pieces of C-$Yb_2Si_2O_7$ crystals selected from H037. The crystals were used for subsequent physical property measurements and neutron scattering experiments [13]. (**i**) The crystal structure of $Yb_2Si_2O_7$ adopting the type-C in the monoclinic space group $C2/m$. The cyan spheres are the Yb, the blue are Si and the red are oxygen. A similar figure for D-$Er_2Si_2O_7$ is shown in (**j**) where the Er atoms are shown in green. In both (**i**,**j**), a unit cell is shown outlined (structure diagrams are prepared using VESTA [17]).

A single attempt to grow $Er_2Si_2O_7$ was conducted, which was successful. Four 1.0 kW halogen lamps were used, and the ceramic feed and seed ingots were observed to melt at 71% lamp voltage but this overheated the melt and the voltage was reduced to 69.6%. The growth was eventually stabilized with a 7 mm/h growth rate, 20 rpm counter rotation of feed and seed rods, and an atmosphere of flowing O_2 gas (350 mL/min). The grown crystal was 3.3 cm long, a cloudy pink color, and was found by Laue X-ray diffraction to contain multiple crystal grains distributed radially, with cracks observed between the different orientations. Since the cracking of the grown crystal was not uniform, breaking the boule resulted in several crystal pieces of different mass and dimensions. $Er_2Si_2O_7$ was 0.12 g (7 mm × 4 mm × 3 mm). These crystal pieces were used for characterizing the physical properties.

3. Powder X-ray Diffraction and Laue

The single crystals of C-$Yb_2Si_2O_7$ and D-$Er_2Si_2O_7$ were characterized first using powder X-ray diffraction methods. Powder diffraction patterns on pulverized crystal pieces were obtained using a Bruker Davinci diffractometer that uses a wavelength, λ = 1.54 Å. The diffraction data was analyzed using Fullprof Suite of programs [18] and Topas Academic [19]. The experimental powder X-ray diffraction patterns of $Yb_2Si_2O_7$ and $Er_2Si_2O_7$ are presented in the panels (a) and (b) respectively in

Figure 3. In the figure, the experimentally recorded data is represented in red circles. The diffraction pattern of $Yb_2Si_2O_7$ was analyzed using the structural model of C-type $R_2Si_2O_7$ in $C2/m$ space group setting [20]. An excellent agreement (χ^2 = 1.62) between the experiment and the structural model (black solid line) is obtained as can be seen from the difference curve that is plotted in blue in the figure. In Figure 3a, some of the peaks are shown indexed in the $C2/m$ structure. In pane Figure 3b, the diffraction pattern of $Er_2Si_2O_7$ is presented along with the analysis using D-type structure in $P2_1/b$ space group (χ^2 = 2.39). A preferred orientation term as well as a "surface roughness correction" of Plitschke type was essential in the refinements to obtain a faithful fit. In the case of $Yb_2Si_2O_7$, the direction of preferred orientation was (110) and for $Er_2Si_2O_7$ it was (001) and (110). From our structural analysis, C-type structure for $Yb_2Si_2O_7$ and D-type for $Er_2Si_2O_7$ are confirmed. In addition, no impurity peaks are observed in the X-ray diffraction patterns signifying the purity of the crystals grown using the floating zone method.

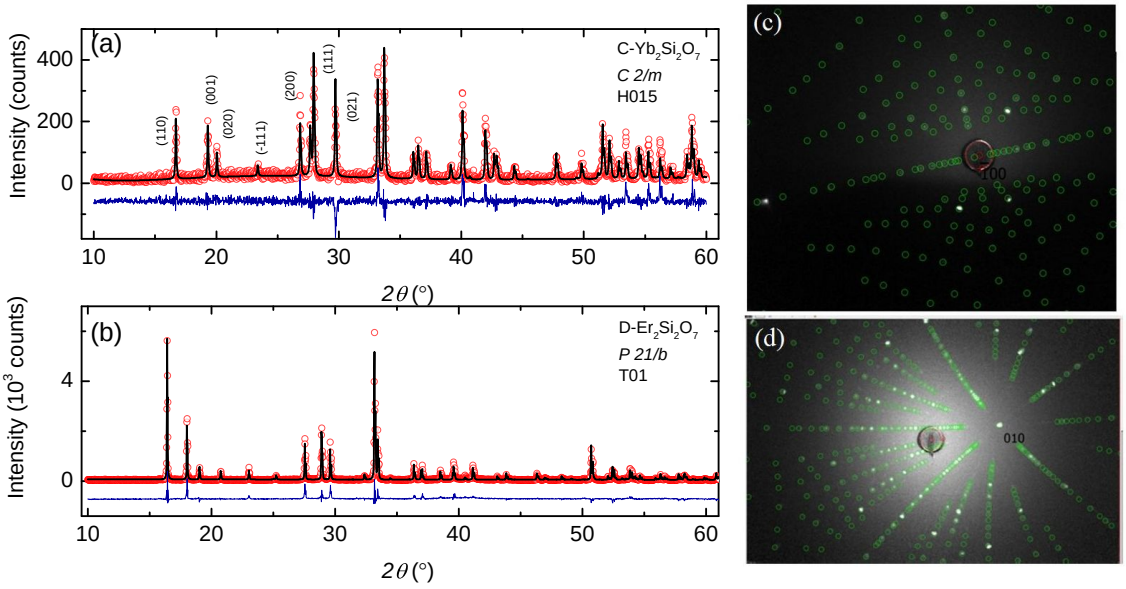

Figure 3. (**a**) The powder X-ray diffraction pattern obtained by pulverizing the single crystals of $Yb_2Si_2O_7$ obtained from the batch H015. After Rietveld refinements, the crystal structure was confirmed as belonging to the space group $C2/m$ (C-type). (**b**) The powder X-ray diffraction pattern belonging to $Er_2Si_2O_7$ (T01 batch) in $P2_1/b$. The tendency of the crystals to crack along specific planes required the use of preferred orientation corrections to the fitted powder patterns in both cases: (001) and (011) for $Er_2Si_2O_7$ and (110) for $Yb_2Si_2O_7$. (**c**) The indexed Laue photograph of $Yb_2Si_2O_7$ along the (100) direction and $Er_2Si_2O_7$ along the (010) direction, (**d**). In (**c**,**d**) the green circles are the calculated Laue spots determined from the corresponding symmetry in each case.

The panels (c) and (d) of Figure 3 shows the Laue photographs obtained on crystal pieces of $Yb_2Si_2O_7$ and $Er_2Si_2O_7$ extracted from the grown crystal boules. The patterns are representative of Laue patterns obtained on several pieces belonging to H015, H037, H045 and T01. The Laue photographs were recorded using a Photonics Science X-ray Laue camera equipped with a CCD screen. The recorded Laue patterns were analyzed using the software, *clip* (Cologne Laue Indexation Program) [21]. Through the indexation of the patterns we identified the (100), (010) and (001) crystallographic directions of both C-$Yb_2Si_2O_7$ and D-$Er_2Si_2O_7$. Shown in panels (c) and (d) are the (100) orientation of C-$Yb_2Si_2O_7$ and (010) orientation of D-$Er_2Si_2O_7$. It was noted that the cracks between the crystals in the multi-crystal boules of $Yb_2Si_2O_7$ tended to be (110) planes. The green circles in the figures are the allowed Laue spots predicted for the space group symmetry in each case, for that particular crystallographic direction (Table 2).

Table 2. Crystal structure parameters of C-$Yb_2Si_2O_7$ in the monoclinic $C2/m$ space group setting are presented in the top section of the table. In the subsequent section, the structural parameters of D-$Er_2Si_2O_7$ in $P2_1/b$ space group are provided. In the bottom two sections, the lattice parameters obtained through Rietveld refinement of powder X-ray data from pulverized crystals in the present case are shown compared to the values from the literature. P: powder, SC: single crystals, PC: powdered crystal, SXRD: synchrotron X-ray diffraction, C: ceramics.

	C-$Yb_2Si_2O_7$	**Wyckoff Pos.**	**x**	**y**	**z**	
	Yb	4*g*	0.5	0.8069	0.0	
	Si	4*i*	0.7189	0.5	0.4125	
	O(1)	2*c*	0.5	0.5	0.5	
	O(2)	4*i*	0.8831	0.5	0.7151	
	O(3)	8*j*	0.7361	0.6504	0.2197	
	D-$Er_2Si_2O_7$	**Wyckoff Pos.**	**x**	**y**	**z**	
	Er	4*e*	0.8897	0.0908	0.3487	
	Si	4*e*	0.3614	0.6511	0.3889	
	O(1)	2*d*	0.5	0.5	0.5	
	O(2)	4*e*	0.2052	0.8653	0.4486	
	O(3)	4*e*	0.1235	0.4583	0.3191	
	O(4)	4*e*	0.6184	0.7522	0.2984	
C-$Yb_2Si_2O_7$	**a (Å)**	**a (Å)**	**a (Å)**	**β (°)**	**Ref.**	**Phase**
$C2/m$	6.876	8.974	4.720	101.8	[5]	P
	6.7991	8.8734	4.7084	101.969	[12]	SC
	6.8005	8.8750	4.7074	101.984	[11]	P
	6.7714(9)	8.8394(2)	4.6896(5)	101.984(9)	[13]	PC, SXRD
	6.7997(9)	8.875(8)	4.7088(5)	101.98(9)	[present work]	PC
D-$Er_2Si_2O_7$	**a (Å)**	**a (Å)**	**a (Å)**	**β (°)**	**Ref.**	**Phase**
$P21/b$	4.683	5.56	10.79	96	[8]	SC
	4.666	5.55	10.81	96	[9]	C
	4.6893(1)	5.5601(8)	10.7967(1)	96.03(2)	[present work]	PC

4. Specific Heat of C-$Yb_2Si_2O_7$ and D-$Er_2Si_2O_7$

The specific heat of $Yb_2Si_2O_7$ and $Er_2Si_2O_7$ (Figure 4) were measured using a dilution refrigerator insert and the specific heat option available with the Quantum Design DynaCool Physical Property Measurement System (PPMS). The specific heat of a crystal of $Yb_2Si_2O_7$ was measured from 50 mK–3 K in an applied field of 0.8 T oriented along the *c* axis. A broad peak is observed at approximately 1 K with a sharp anomaly at 250 mK, which signals the onset of field-induced magnetic order in this quantum dimer magnet. Note that these data, as well as data collected at additional field strengths, are also shown and discussed in detail in Ref. [13].

The specific heat of a D-$Er_2Si_2O_7$ crystal was measured from 1.3–2.5 K in zero field, revealing a sharp λ-like feature at 1.8 K. The magnetic properties of the D-$Er_2Si_2O_7$ powders reported previously showed a rather broad magnetic phase transition occurring at $T_N = 1.9 \pm 0.1$ K determined originally from the point of maximum slope in the magnetic susceptibility data [8]. Magnetic susceptibilities measured along different crystallographic directions in a single crystal yielded the *g*-tensors, $g_{\parallel} = 12.2$, $g_{\perp} = 2.0$ and g_c (along *c*-axis) = 4.7 indicating the approximate Ising antiferromagnetic nature of D-$Er_2Si_2O_7$ [8]. The above-reported magnetic transition is reflected in our specific heat measurements as a λ-like peak at 1.8 K. Note that in the case of C-type $Er_2Si_2O_7$, the magnetic phase transition occurs at $T_N = 2.50$ K [6,7]. The observed phase transition temperature in the present sample of $Er_2Si_2O_7$ further confirms that the structure type is indeed D-type. Given that the Kramers ion Er^{3+} forms an effective $S = 1/2$ doublet in crystal field environments with low enough symmetry, it is expected that D-$Er_2Si_2O_7$ could be a candidate for a quantum phase transition resulting from the

application of a magnetic field transverse to the Ising axis. This will be a topic for future study of these crystals.

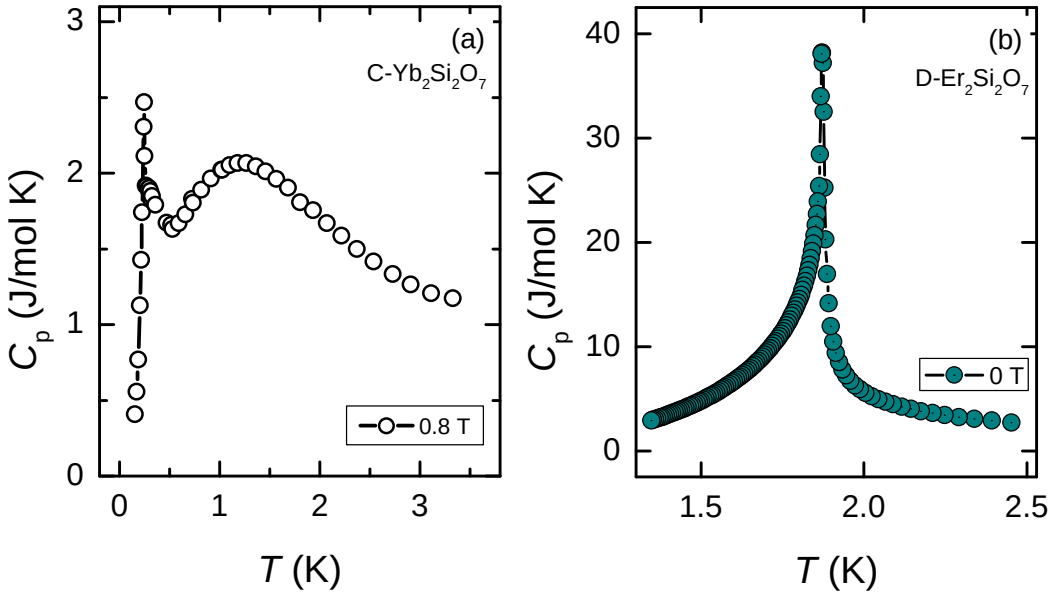

Figure 4. (**a**) The specific heat, $C_p(T)$ of C-$Yb_2Si_2O_7$ measured in the temperature range of 50 mK to 3 K in 0.8 T external magnetic field oriented along c, evealing a broad feature peaked at ≈1 K and a sharp anomaly at 250 mK. (**b**) Shows the $C_p(T)$ of D-$Er_2Si_2O_7$ in zero magnetic field. A sharp λ-like phase transition is visible at 1.8 K.

5. Conclusions

Using the method of optical floating zone melting, we have successfully prepared single crystals of rare-earth pyrosilicates C-$Yb_2Si_2O_7$ and D-$Er_2Si_2O_7$. Large crystal boules have been prepared. However, in the case of both C-$Yb_2Si_2O_7$ and D-$Er_2Si_2O_7$, cracking of the crystals occurred post crystal growth in the furnace as the result of multi-crystal formation. In our growth trials, transparent, good quality C-$Yb_2Si_2O_7$ was obtained by using a growth rate of 3 mm/h and by keeping an oxygen pressure of 1 atm in the growth chamber. In comparison, the growth of D-$Er_2Si_2O_7$ produced pink crystals with a 7 mm/h growth rate, 1 atm oxygen pressure and 0.35 L/min flow in the growth chamber. Through X-ray diffraction and Laue photography we have characterized the crystal structure of both $Yb_2Si_2O_7$ and $Er_2Si_2O_7$ and ascertained that they belong to the C- and D-type respectively. The physical properties of both the compounds were studied using low temperature specific heat measurements. We found field-induced magnetic order at 250 mK in a field of 0.8 T in C-$Yb_2Si_2O_7$, as well as an antiferromagnetic transition at 1.8 K in D-$Er_2Si_2O_7$. The crystals of $Yb_2Si_2O_7$ and $Er_2Si_2O_7$ obtained by the optical floating zone method are of suitable size and quality to be studied by inelastic neutron scattering, which will enable a full investigation of their quantum magnetic properties.

Author Contributions: Conceptualization, K.A.R.; resources, K.A.R.; writing—original draft preparation, H.S.N.; investigation, H.S.N., T.D., T.R., A.S., G.H.; writing—review and editing, K.A.R.; supervision, H.S.N., K.A.R.; funding acquisition, K.A.R.

Funding: This research was partially funded by the National Science Foundation, grant number DMR-1611217.

Acknowledgments: We acknowledge the contributions of the Neilson laboratory at CSU in the initial stages of our work on the rare-earth pyrosilicates, contributions from A. Glock in preparing starting materials, as well as the the use of equipment in the Central Instrument Facility at CSU.

Conflicts of Interest: The authors declare no conflict of interest.

Abbreviations

The following abbreviations are used in this manuscript:

FZ	Floating zone
TSFZ	Traveling solvent floating zone
CCD	Charge coupled device

References

1. Felsche, J. The crystal chemistry of the rare-earth silicates. In *Rare Earths*; Springer: New York, NY, USA, 1973; pp. 99–197.
2. Feng, H.; Ding, D.; Li, H.; Lu, S.; Pan, S.; Chen, X.; Ren, G. Growth and luminescence characteristics of cerium-doped yttrium pyrosilicate single crystal. *J. Alloys Compd.* **2010**, *489*, 645–649. [CrossRef]
3. Pauwels, D.; Le Masson, N.; Viana, B.; Kahn-Harari, A.; van Loef, E.; Dorenbos, P.; van Eijk, C. A novel inorganic scintillator: $Lu_2Si_2O_7$: Ce^{3+}. *IEEE Trans. Nucl. Sci.* **2000**, *47*, 1787–1790. [CrossRef]
4. Bretheau-Raynal, F.; Tercier, N.; Blanzat, B.; Drifford, M. Synthesis and spectroscopic study of lutetium pyrosilicate single crystals doped with trivalent europium. *Mater. Res. Bull.* **1980**, *15*, 639–646. [CrossRef]
5. Luo, Y.; Sun, L.; Wang, J.; Wu, Z.; Lv, X.; Wang, J. Material-genome perspective towards tunable thermal expansion of rare-earth di-silicates. *J. Eur. Ceram. Soc.* **2018**, *38*, 3547–3554. [CrossRef]
6. Maqsood, A.; Wanklyn, B.M.; Garton, G. Flux growth of polymorphic rare-earth disilicates, $R_2Si_2O_7$ (R = Tm, Er, Ho, Dy). *J. Cryst. Growth* **1979**, *46*, 671–680. [CrossRef]
7. Maqsood, A. Single crystal growth of polymorphic $Er_2Si_2O_7$ ceramics. *J. Mater. Sci. Lett.* **2000**, *19*, 711–712. [CrossRef]
8. Maqsood, A. Magnetic properties of D-$Er_2Si_2O_7$ at low temperatures. *J. Mater. Sci.* **1981**, *16*, 2198–2204. [CrossRef]
9. Maqsood, A. Phase transformations in $Er_2Si_2O_7$ ceramics. *J. Mater. Sci. Lett.* **1997**, *16*, 837–840. [CrossRef]
10. Wang, S.B.; Lu, Y.R.; Chen, Y.X. Synthesis of single-phase β-$Yb_2Si_2O_7$ and properties of its sintered bulk. *Int. J. Appl. Ceram. Technol.* **2015**, *12*, 1140–1147. [CrossRef]
11. Zhao, C.; Wang, F.; Sun, Y.; Zhou, Y. Synthesis and characterization of β-$Yb_2Si_2O_7$ powders. *Ceram. Int.* **2013**, *39*, 5805–5811. [CrossRef]
12. Horiai, T.; Kurosawa, S.; Murakami, R.; Pejchal, J.; Yamaji, A.; Shoji, Y.; Chani, V.I.; Ohashi, Y.; Kamada, K.; Yokota, Y.; et al. Crystal growth and luminescence properties of $Yb_2Si_2O_7$ infra-red emission scintillator. *Opt. Mater.* **2016**, *58*, 14–17. [CrossRef]
13. Hester, G.; Nair, H.; Reeder, T.; Yahne, D.; DeLazzer, T.; Berges, L.; Ziat, D.; Quilliam, J.; Neilson, J.; Aczel, A.; et al. A novel strongly spin-orbit coupled quantum dimer magnet: $Yb_2Si_2O_7$. *arXiv* **2018**, arXiv:1810.13096.
14. Pidol, L.; Viana, B.; Galtayries, A.; Dorenbos, P. Energy levels of lanthanide ions in a $Lu_2Si_2O_7$ host. *Phys. Rev. B* **2005**, *72*, 125110. [CrossRef]
15. Ogawa, T.; Kobayashi, S.; Wada, M.; Fisher, C.A.; Kuwabara, A.; Kato, T.; Yoshiya, M.; Kitaoka, S.; Moriwake, H. Isolated energy level in the band gap of $Yb_2Si_2O_7$ identified by electron energy-loss spectroscopy. *Phys. Rev. B* **2016**, *93*, 201107. [CrossRef]
16. Koohpayeh, S.M. Single crystal growth by the traveling solvent technique: A review. *Prog. Cryst. Growth Charact. Mater.* **2016**, *62*, 22–34. [CrossRef]
17. Momma, K.; Izumi, F. VESTA 3 for three-dimensional visualization of crystal, volumetric and morphology data. *J. Appl. Crystallogr.* **2011**, *44*, 1272–1276. [CrossRef]
18. Rodriguez-Carvajal, J. Fullprof Suite. Available online: http://www.ill.eu/sites/fullprof/ (accessed on 2 April 2019).
19. Coelho, A.A. TOPAS and TOPAS-Academic: an optimization program integrating computer algebra and crystallographic objects written in C++. *J. Appl. Crystallogr.* **2018**, *51*, 210–218. [CrossRef]

20. Bretheau-Raynal, F.; Lance, M.; Charpin, P. Crystal data for $Lu_2Si_2O_7$. *J. Appl. Crystallogr.* **1981**, *14*, 349–350. [CrossRef]
21. Cologne Laue Indexation Program. clip4. Available online: http://clip4.sourceforge.net/ (accessed on 2 April 2019).